

**Multifunctional Charge and Hydrogen-Bond Effects of Second-Sphere
Imidazolium Pendants Promote Capture and Electrochemical Reduction of
CO₂ in Water Catalyzed by Iron Porphyrins**

Mina R. Narouz,^[a,b] Patricia De La Torre,^[a,b] Lun An,^[a,b] Christopher J. Chang^{[a,b,c]}*

^[a] Department of Chemistry, University of California, Berkeley, CA 94720-1460 (USA)

^[b] Chemical Sciences Division, Lawrence Berkeley National Laboratory, Berkeley, CA 94720-
1460 (USA)

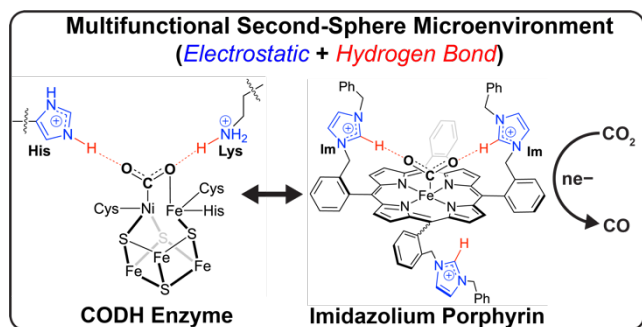
^[c] Department of Molecular and Cell Biology, University of California, Berkeley
Berkeley, CA 94720-1460 (USA)

*Corresponding author: chrischang@berkeley.edu

Table of Contents Synopsis

Iron porphyrins decorated with imidazolium (im) pendants enable the disentangling of second-sphere contributions that stem from through-space charge and hydrogen-bond interactions for the electrochemical CO₂ reduction reaction (CO₂RR). Synergistic through-space electrostatic and hydrogen-bond effects in **Fe-ortho-im(H)** lead to a 25-fold increase in CO₂ affinity and 2,000-fold increase in CO₂RR activity over parent Fe-TPP. Charge effects are the dominant contributor to observed improvements in CO₂ conversion with hydrogen bonding effects augmenting CO₂ capture affinity, resulting effective homogeneous electrocatalytic CO₂RR in water.

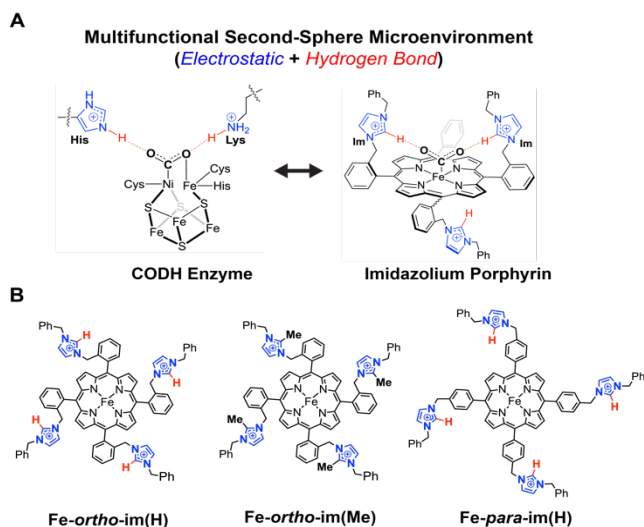
Table of Contents Graphic



ABSTRACT: Microenvironments tailored by multifunctional secondary coordination sphere groups can enhance catalytic performance at primary metal active sites in natural systems. Here, we capture this biological concept in synthetic systems by developing a family of iron porphyrins decorated imidazolium (im) pendants for the electrochemical CO₂ reduction reaction (CO₂RR), which promotes multiple synergistic effects to enhance CO₂RR and enables the disentangling of second-sphere contributions that stem from each type of interaction. **Fe-ortho-im(H)**, which poises imidazolium units featuring both positive charge and hydrogen-bond capabilities proximal to the active iron center, increases CO₂ binding affinity by 25-fold and CO₂RR activity by 2,000-fold relative to the parent Fe tetraphenylporphyrin (Fe-TPP), achieving turnover frequencies (TOF) exceeding 10⁹ s⁻¹ with >95% Faradaic efficiency for CO product. Owing to these dual, synergistic second-sphere enhancements, this catalyst also retains high activity and selectivity for homogeneous CO₂RR in aqueous media. Notably, the observed TOF value for **Fe-ortho-im(H)** is 14,000-fold higher than the **Fe-para-im(H)** positional analog, but only 40-fold higher than the **Fe-ortho-im(Me)** congener that retains the proximal positive charge but lacks the C2-H hydrogen-bonding moiety, revealing that through-space charge effects have a greater impact on catalytic CO₂RR performance compared to hydrogen bonding in this context. This work emphasizes the use of second-sphere pendants that can promote multiple synergistic effects as a design strategy for achieving CO₂ reduction catalysis in water.

Rising global energy demands and fossil fuel use contribute to increasing concentrations of atmospheric carbon dioxide (CO₂).^[1] Capture and electrochemical reduction of CO₂ offers a potentially powerful approach to converting this greenhouse gas into value-added chemical products.^[2] The electrochemical CO₂ reduction reaction (CO₂RR) faces high kinetic and thermodynamic barriers, making it challenging to achieve requisite selectivity and activity,

especially in aqueous media, where the abundance of protons favor the competing hydrogen evolution reaction (HER).^[3] In this regard, enzyme biocatalysts such as Ni-Fe carbon monoxide dehydrogenases (CODH), enable the interconversion of CO₂ and CO near the thermodynamic potential in neutral pH water^[4] and provide inspiration for development of synthetic systems that can functionally mimic their chemistry.^[2g, 3c]



Scheme 1. (A) Multifunctional histidine (His) and lysine (Lys) second-sphere protein residues proximal to the Fe-Ni cluster active site in the natural CODH biocatalyst inspire the design of synthetic Fe porphyrin catalysts decorated with multifunctional imidazolium pendants. (B) Fe porphyrins synthesized in this work enable disentangling of relative contributions of through-space electrostatic and C2-H hydrogen-bond interactions and positioning of second-sphere groups.

In particular, Ni-Fe CODH provides a microenvironment with a tailored secondary coordination sphere featuring two key histidine imidazolium (His₉₃) and lysine (K₅₆₃) ammonium pendants that are positioned proximally to the redox-active iron-sulfur cluster active site (Scheme 1A). These multifunctional second-sphere groups work in concert to help stabilize CO₂-bound intermediates via both through-space electrostatic and hydrogen-bond interactions.^[5] We now

report that this concept can be captured in synthetic systems through the development of a family of iron porphyrins bearing multifunctional imidazolium pendants in the secondary coordination sphere (Scheme 1B). Combined electrostatic and hydrogen-bond interactions in **Fe-ortho-im(H)** result in enhanced CO₂ binding and fast and selective electrochemical CO₂ conversion in both organic and aqueous media, with a 2,000-fold increase in CO₂RR activity relative to the parent Fe tetraphenylporphyrin (Fe-TPP) compound.^[6] Comparison with the **Fe-ortho-im(Me)** analog that retains the charged functionality but lacks the C2-H hydrogen-bond moiety indicates that while hydrogen-bonding enhances CO₂ capture, the proximal electrostatic component contributes the majority of the catalytic amplification observed in this system. This work establishes the use of multifunctional second-sphere pendants as an effective strategy for enhancing the performance of synthetic electrocatalysts and emphasizes the importance of disentangling relative contributions of second-sphere functionalities to inform catalyst design.

Table 1. Electrochemical properties of iron porphyrin catalysts.

| Catalyst | E_{cat}^o [a] | KCO ₂ [b] | LogTOF _{max} [c] | KIE [d] | FE _{CO} [e] |
|------------------------|-----------------|----------------------|---------------------------|---------|----------------------|
| Fe-ortho-im(H) | -1.78 | 65 | 9.1 | 8.7 | 100 |
| Fe-ortho-im(Me) | -1.79 | 12 | 7.5 | 9.2 | 100 |
| Fe-para-im(H) | -1.79 | 3 | 4.9 | 6.5 | 28 |
| FeTPP | -2.06 | 2.58 | 5.8 | — | 98 |

[a] E_{cat}^o (V vs. Fc⁺/Fc) obtained from CVs under argon and catalyst concentration (0.3 mM). [b] K_{CO₂} (M⁻¹) data was obtained from measuring CVs under a CO₂ atmosphere without 2,2,2-trifluoroethanol (TFE) at a scan rate of 1.0 V s⁻¹. [d] Kinetic isotope effect (KIE) values represent the ratio of k_H/k_D measured using water as the proton source. [c] Maximum turnover frequency (TOF_{max}) values were estimated using foot-of-the-wave (FOWA) under CO₂ with 3.0 M TFE. [e] FE (%) data for CO was obtained as an average of three controlled potential electrolyses (CPEs) under CO₂ with 1.5 M TFE and catalyst concentration (10 μM). All

experiments in this table were performed in 0.1 M tetrabutylammonium hexafluorophosphate (TBAPF₆)/MeCN, conditions used for FeTPP are provided in the reference.

In contrast to what is observed for natural CO₂RR biocatalysts, advances in synthetic CO₂RR catalysts have largely focused on monofunctional second-sphere pendants,^[7] including privileged Fe porphyrin scaffolds incorporating hydrogen-bonding groups such as phenols,^[7a, 7c, 8] amides,^[7e, 9] ureas,^[7j, 7m, 7p, 10] guanidines,^[11] and triazoles,^[7i, 12] or through-space electrostatic functionalities such as trimethylanilinium^[7d, 13] or imidazolium^[7q, 14] cations. In this context, we reasoned that imidazoliums, when properly positioned, could serve as multifunctional second-sphere pendants that induce both through-space electrostatic and hydrogen-bonding effects, as well as offer the potential to disentangle the contributions that each type of functionality plays. Indeed, Nippe and colleagues reported that tethering of an imidazolium group improved activity in metal tricarbonyl-bipyridine CO₂RR catalysts^[15] and Aukauloo and colleagues observed through-space charge enhancement for CO₂RR in iron porphyrins linked to distal imidazolium pendants through an aryl amide spacer.^[7q, 14] Against this backdrop, we designed and synthesized a family of tetracationic imidazolium porphyrins that enabled systematic evaluation of positional tuning as well as hydrogen-bonding and through-space charge contributions. Specifically, we prepared C2-H and C2-methyl imidazolium (im) units at either the ortho [**Fe-ortho-im(H)**, **Fe-ortho-im(Me)**] or para [**Fe-para-im(H)**] positions on the ancillary phenyl rings of a tetraphenylporphyrin scaffold (Scheme 1B). The target catalysts were synthesized in high yield in three steps, starting from appropriate ortho or para-(bromomethyl)benzaldehyde precursors (Scheme S1). **Fe-ortho-im(H)** places imidazolium units proximal to the Fe center to deliver both hydrogen-bond and charge stabilization functionalities to CO₂-bound intermediates. In **Fe-ortho-im(Me)**, the C2-H units are blocked with methyl groups to probe how through-space electrostatic effects alone influence

CO₂RR catalysis. Finally, the **Fe-*para*-im(H)** was synthesized to evaluate positional effects of the secondary imidazolium unit relative to the primary Fe center. Interestingly, incorporating imidazolium groups into the metalloporphyrin scaffold affords solubility in water, acetonitrile (MeCN), and dimethylformamide (DMF) (Figures S30-31, 33), in contrast to the vast majority of porphyrins whose solubility restricts their use as homogeneous electrocatalysts in DMF. [6-7, 7d, 7e, 7m, 7q, 14]

The redox behaviors of **Fe-*ortho*-im(H)**, **Fe-*ortho*-im(Me)**, and **Fe-*para*-im(H)** were characterized using cyclic voltammetry (CV) measurements in MeCN under an argon (Ar) atmosphere. The CVs show three distinct redox events corresponding to formal Fe^{III/II}, Fe^{II/I}, and Fe^{I/0} couples (Figure 1, Table S1). Scan rate-dependent data show a linear correlation between the peak current of the Fe^{I/0} couples and the square root of the scan rate, indicating that all catalysts are freely diffusible under non-catalytic conditions (Figure S1). The observed formal Fe^{I/0} potentials, E_{cat}^o , of the three porphyrins are similar (ca. -1.8 V vs. Fc⁺/Fc), indicating that the electronic properties of all members of this series are comparable. There is a 276 mV positive shift

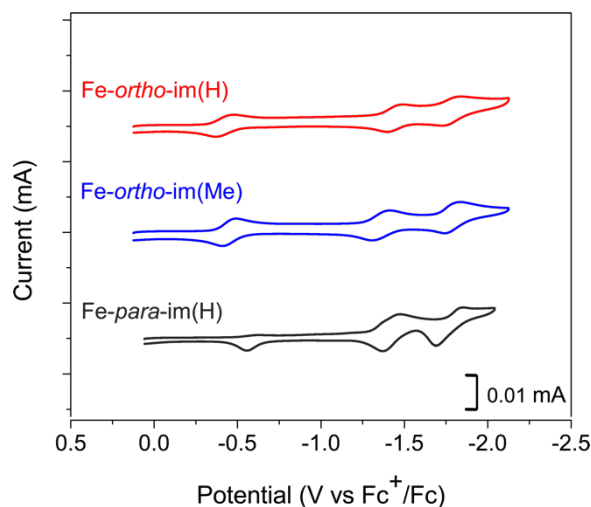


Figure 1. Cyclic voltammograms (CVs) of imidazolium (im)-functionalized porphyrins under Ar. Conditions: 0.3 mM catalyst, 0.1 M TBAPF₆ in MeCN; scan rate is 100 mV s⁻¹.

in the $\text{Fe}^{I/0}$ couple relative to the parent catalyst $\text{Fe-TPP}^{[6]}$ (Table S1), presaging that the cationic imidazolium units could activate CO_2 at lower potentials, presumably by electrostatic stabilization of reduced iron species. Next, in order to decipher hydrogen-bond and through-space charge contributions in promoting CO_2 capture prior to evaluation of CO_2RR catalysis, we estimated the CO_2 binding constants (K_{CO_2}) by measuring the shift in the $\text{Fe}^{I/0}$ wave under Ar and CO_2 atmospheres in the absence of a proton source to prevent subsequent catalytic turnover (Table 1 and Figure S2). **Fe-ortho-im(H)** exhibits a K_{CO_2} value of 65 M^{-1} , representing a 5-fold increase in CO_2 binding affinity over **Fe-ortho-im(Me)** and a 20-fold increase over **Fe-para-im(H)**, suggesting that both through-space electrostatic and hydrogen-bonding interactions in the proximal ortho position stabilize the Fe-CO_2 adduct.

Upon addition of 2,2,2-trifluoroethanol (TFE) as a proton source, all three Fe porphyrins show large catalytic current enhancement under a CO_2 atmosphere, with **Fe-ortho-im(H)** showing

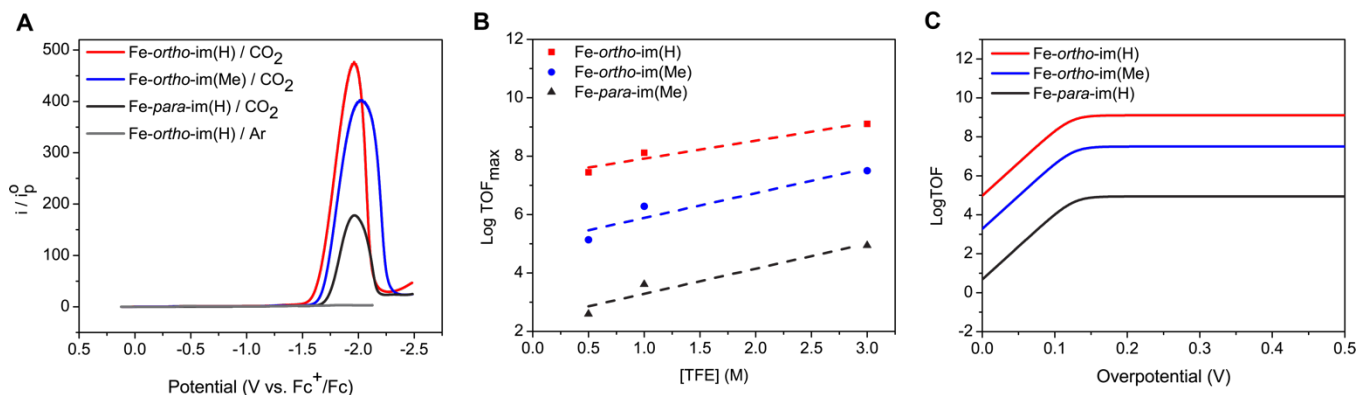


Figure 2. Cyclic voltammetry (CV) experiments. CVs of imidazolium (im)-functionalized porphyrins under (A) CO_2 in the presence of 3 M TFE. (B) Calculated $\text{logTOF}_{\text{max}}$ as a function of TFE concentration. (C) Catalytic Tafel plots. Conditions: 0.3 mM catalyst, 0.1 M TBAPF₆ in MeCN; scan rate is 100 mV s^{-1} . i_p^0 represents the cathodic peak height of the formal $\text{Fe}^{II/I}$ couple under Ar. TOF_{max} values were determined by FOWA (see SI for details).

the highest catalytic current and most positive onset potential for catalysis, followed by **Fe-ortho-im(Me)**, with **Fe-para-im(H)** being the least active of the three congeners (Figure 2A, S3). To estimate the turnover frequency (TOF) values free from secondary phenomena (e.g., substrate consumption, product inhibition, catalyst degradation), we applied the foot-of-the-wave analysis (FOWA) introduced by Savéant and colleagues (Tables 1, S2, S3, Figure S4).^[7d, 16] We observed a linear relationship between $\text{LogTOF}_{\text{max}}$ values and the concentration of added TFE (Figure 2B), demonstrating that the rates display a first-order dependence on the acid concentration. The observed TOF values with 3.0 M TFE for the **Fe-ortho-im(H)** catalyst ($1.3 \times 10^9 \text{ s}^{-1}$) represent a 14,000-fold increase over the positional **Fe-para-im(H)** congener ($8.7 \times 10^4 \text{ s}^{-1}$) and 2,000-fold increase over Fe-TPP-ClO₄ in MeCN ($6.5 \times 10^5 \text{ s}^{-1}$),^[6] but only a 40-fold increase over the **Fe-ortho-im(Me)** derivative ($3.2 \times 10^7 \text{ s}^{-1}$) that retains the imidazolium positive charge but lacks the C2-H hydrogen-bond capability. The data indicate that electrostatic effects dominate catalytic amplification over hydrogen-bond interactions in this context.

We next moved on to construct catalytic Tafel plots in which the LogTOF values vary as a function of applied overpotential, where the most efficient electrocatalysts function with high TOFs at low overpotentials. The three catalysts reach a plateau ($\text{LogTOF}_{\text{max}}$) at relatively low overpotentials (ca. 0.15 V, Figure 2C), with **Fe-ortho-im(H)** exhibiting higher TOFs over all applied potentials relative to its congeners. Benchmarking^[17] **Fe-ortho-im(H)**, **Fe-ortho-im(Me)**, and **Fe-para-im(H)** indicates that **Fe-ortho-im(H)** is among the fastest homogeneous molecular catalysts for electrochemical CO₂RR reported to date (Table S3 and Figures S5, S6). In addition, to determine the contributions of proton transfer in CO₂RR catalysis, we measured kinetic isotope effects (KIE) for all three catalysts using varying concentrations of H₂O or D₂O as the proton source (Table 1, Figures S7-15). Large normal primary KIEs were observed for all three catalysts

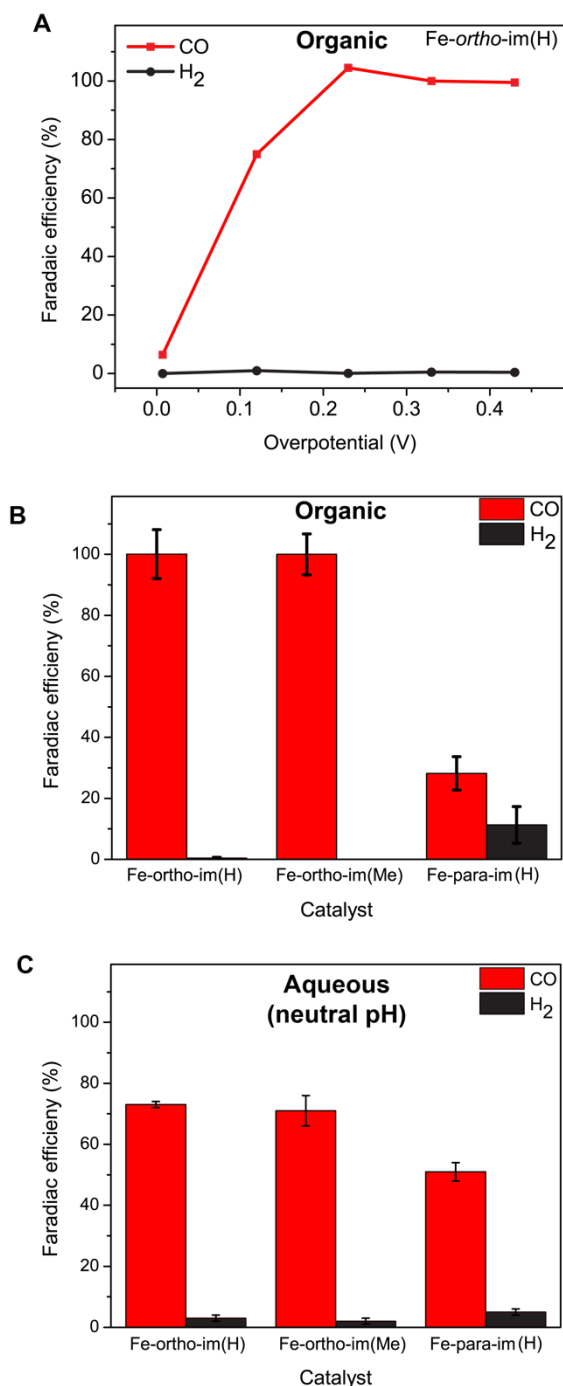


Figure 3. Controlled-potential electrolysis (CPE) experiments. (A) Faradaic efficiencies as a function of overpotential in CPE experiment using **Fe-ortho-im(H)** in 0.1 M TBAPF₆ in MeCN; overpotential values are reported as the difference between the E_{cat}^O and $E_{CO_2/CO}^O = -1.54$ vs. Fc⁺/Fc for MeCN. CPEs of imidazolium-functionalized porphyrins under CO₂ (B) at -1.87 V (vs. Fc⁺/Fc) in 0.1 M TBAPF₆ in MeCN and (C) in 0.1 M aqueous PBS (pH of 6.8). Catalyst concentration in all CPEs (10 μM). (See SI for details).

(6.5 to 9.2), suggesting that proton transfer is involved in the rate-determining step regardless of imidazolium positioning.

With data in hand showing that these second-sphere imidazolium pendants promote enhanced CO₂RR activity, we then performed controlled potential electrolysis (CPE) experiments to measure catalyst stability and product distribution. CPE measurements were conducted in a CO₂-saturated NBu₄PF₆/MeCN electrolyte using a glassy carbon electrode with as low as 10 μM catalyst loading (Figures 3, S16). **Fe-ortho-im(H)** is highly selective for CO₂RR over HER, generating CO as a product over a wide potential range with Faradaic efficiencies (FE) that exceed 95% at overpotentials^[6, 18] above 0.2 V (Figures 3A, S17). CPEs at -1.87 V vs. Fc+/Fc ($\eta = 0.3$ V) showed that both **Fe-ortho-im(H)** and **Fe-ortho-im(Me)** were selective towards CO production (FE \approx 100%) with more charge passed using **Fe-ortho-im(H)**, whereas **Fe-para-im(H)** shows a significant loss in selectivity for CO production (FE \approx 28%). (Tables 1, S4, Figures 3B, S18-19).

Observing that the cationic nature of the imidazolium pendants enabled solubility of these catalysts in water (Figures S29-30, 32), we next proceeded to evaluate their performance for homogeneous electrochemical CO₂RR in aqueous media. We were pleased to find that both **Fe-ortho-im(H)** and **Fe-ortho-im(Me)** exhibit exceptionally high rates for CO₂RR in aqueous KCl solution, with TOF_{max} values of 4.6×10^6 and 2.3×10^6 , respectively (Figures S21-22, Table S5). The **Fe-para-im(H)** complex was not sufficiently soluble under these conditions for evaluation. The observed TOF value of **Fe-ortho-im(H)** is only 2-fold higher than that of **Fe-ortho-im(Me)**, confirming that through-space charge effects dominate over hydrogen-bonding ones these imidazolium systems. Moreover, CPE experiments under CO₂ in 0.1 M KCl electrolyte (initial pH of 4.0) showed that both **Fe-ortho-im(H)** and **Fe-ortho-im(Me)** catalysts retained their high selectivity for CO₂RR over HER, even in aqueous media with an abundance of protons, with FE

> 90% for CO product (Figure S23, Table S6). Additionally, we performed CPE experiments in aqueous phosphate solutions buffered to near neutral pH (6.8), where all three catalysts were soluble. The **Fe-ortho-im(H)** and **Fe-ortho-im(Me)** complexes were again more selective for CO formation (FE 70%) compared to **Fe-para-im(H)** counterpart (FE 50%), with <5% H₂ evolution

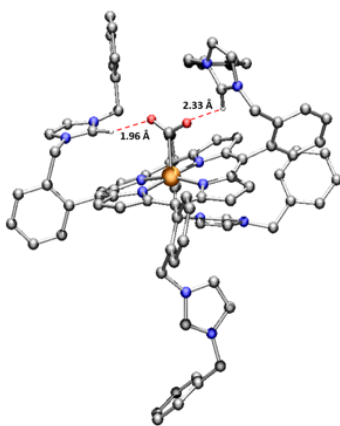


Figure 4. Density-functional tight-binding (DFTB)-optimized structure of the [Fe–CO₂]²⁻ adduct on **Fe-ortho-im(H)**. Hydrogen atoms and bromides were omitted for clarity except for the C1 imidazolium hydrogens. H white, C grey, N blue, O red; Fe orange.

observed for all three catalysts, even in aqueous conditions with an abundance of available protons (Figures 3C, S24, Table S7). Interestingly, these data indicate that imidazolium groups are superior at suppressing HER compared to related cationic anilinium Fe-porphyrin catalysts under similar conditions, where the latter systems show ca. 50% FE for H₂ production in water. ^[8d]

To close, we have presented a family of iron porphyrins functionalized with multifunctional imidazolium pendants in the secondary coordination sphere. These pendants promote synergistic through-space electrostatic and hydrogen-bonding interactions to improve activity and selectivity for homogeneous electrochemical CO₂RR, as well as enable us to disentangle contributions for each of these individual second-sphere effects. Specifically,

comparison of **Fe-ortho-im(H)** and **Fe-ortho-im(Me)** versus a para-substituted counterpart reveals that while electrostatic effects contribute a majority of the observed catalytic enhancements, synergistic hydrogen-bonding effects further augment CO₂ capture affinity and CO₂RR conversion rates. Indeed, the calculated geometry optimization of the Fe-CO₂ adduct of **Fe-ortho-im(H)** using the density-functional tight-binding (DFTB) method suggests that the imidazolium pendants orient themselves towards the CO₂ ligand and form short-hydrogen bonds between the C2-H groups and bound CO₂ (1.97 and 2.33 Å), reminiscent to what is found in the active site of Ni-Fe CODH enzymes (2.63 and 2.88 Å) (Figures 4, S26).^[8d] This compound, which possesses both electrostatic and hydrogen-bonding capabilities, shows the highest activity and selectivity for CO₂RR in the series, with rate enhancements of 2,000-fold over the parent Fe-TPP compound, enabling efficient, homogeneous CO₂RR in both organic and aqueous media. This work provides a starting point for designing second-sphere pendants that enable synergistic, multifunctional effects to enhance catalytic performance for a broader array of chemical transformations, in particular avoiding competing hydrogen evolution pathways even in proton-rich aqueous media.

ACKNOWLEDGMENTS

This work was supported by the U.S. Department of Energy, Office of Basic Energy Sciences, via the Division of Chemical Sciences, Geosciences, and Bioscience of the U.S. Department of Energy at Lawrence Berkeley National Laboratory (Grant No. DE-AC02-05CH11231 to C.J.C.) M.R.N. acknowledges support from an NSERC (Canada) postdoctoral fellowship and P.D.T. acknowledges NSF for a graduate fellowship. We acknowledge Drs. Kathleen A. Durkin and Dave Small at the Molecular Graphics and Computation Facility (MGCF) (NIH S10OD023532) for their

advice regarding DFTB calculations. We acknowledge the use of CoC-NMR instruments supported in part by NIH S10OD024998. C.J.C. is a CIFAR Fellow.

KEYWORDS: electrochemical carbon dioxide reduction • carbon dioxide capture • second-sphere effect • iron porphyrin • imidazolium

REFERENCES

- [1] A. Kätelhön, R. Meys, S. Deutz, S. Suh, A. Bardow, *Proceedings of the National Academy of Sciences* 2019, 116, 11187-11194.
- [2] a) Y. Hori, in *Modern Aspects of Electrochemistry* (Eds.: C. G. Vayenas, R. E. White, M. E. Gamboa-Aldeco), Springer New York, New York, NY, 2008, pp. 89-189; b) E. E. Benson, C. P. Kubiak, A. J. Sathrum, J. M. Smieja, *Chemical Society Reviews* 2009, 38, 89-99; c) A. M. Appel, J. E. Bercaw, A. B. Bocarsly, H. Dobbek, D. L. DuBois, M. Dupuis, J. G. Ferry, E. Fujita, R. Hille, P. J. A. Kenis, C. A. Kerfeld, R. H. Morris, C. H. F. Peden, A. R. Portis, S. W. Ragsdale, T. B. Rauchfuss, J. N. H. Reek, L. C. Seefeldt, R. K. Thauer, G. L. Waldrop, *Chemical Reviews* 2013, 113, 6621-6658; d) R. Francke, B. Schille, M. Roemelt, *Chemical Reviews* 2018, 118, 4631-4701; e) S. Zhao, R. Jin, R. Jin, *ACS Energy Letters* 2018, 3, 452-462; f) P. D. Luna, C. Hahn, D. Higgins, S. A. Jaffer, T. F. Jaramillo, E. H. Sargent, *Science* 2019, 364, eaav3506; g) A. H. Proppe, Y. C. Li, A. Aspuru-Guzik, C. P. Berlinguette, C. J. Chang, R. Cogdell, A. G. Doyle, J. Flick, N. M. Gabor, R. van Grondelle, S. Hammes-Schiffer, S. A. Jaffer, S. O. Kelley, M. Leclerc, K. Leo, T. E. Mallouk, P. Narang, G. S. Schlau-Cohen, G. D. Scholes, A. Vojvodic, V. W.-W. Yam, J. Y. Yang, E. H. Sargent, *Nature Reviews Materials* 2020, 5, 828-846.
- [3] a) S. Nitopi, E. Bertheussen, S. B. Scott, X. Liu, A. K. Engstfeld, S. Horch, B. Seger, I. E. L. Stephens, K. Chan, C. Hahn, J. K. Nørskov, T. F. Jaramillo, I. Chorkendorff, *Chemical Reviews*

2019, 119, 7610-7672; b) E. Boutin, L. Merakeb, B. Ma, B. Boudy, M. Wang, J. Bonin, E. Anxolabéhère-Mallart, M. Robert, *Chemical Society Reviews* 2020, 49, 5772-5809; c) P. T. Smith, E. M. Nichols, Z. Cao, C. J. Chang, *Accounts of Chemical Research* 2020, 53, 575-587; d) P. Saha, S. Amanullah, A. Dey, *Accounts of Chemical Research* 2022, 55, 134-144.

[4] a) F. A. Armstrong, J. Hirst, *Proceedings of the National Academy of Sciences* 2011, 108, 14049-14054; b) V. C.-C. Wang, S. W. Ragsdale, F. A. Armstrong, *ChemBioChem* 2013, 14, 1845-1851.

[5] a) C. L. Drennan, J. Heo, M. D. Sintchak, E. Schreiter, P. W. Ludden, *Proceedings of the National Academy of Sciences* 2001, 98, 11973-11978; b) J.-H. Jeoung, H. Dobbek, *Science* 2007, 318, 1461-1464.

[6] K. Kosugi, M. Kondo, S. Masaoka, *Angewandte Chemie International Edition* 2021, 60, 22070-22074.

[7] a) C. Costentin, S. Drouet, M. Robert, J.-M. Savéant, *Science* 2012, 338, 90-94; b) J. Y. Yang, S. E. Smith, T. Liu, W. G. Dougherty, W. A. Hoffert, W. S. Kassel, M. R. DuBois, D. L. DuBois, R. M. Bullock, *Journal of the American Chemical Society* 2013, 135, 9700-9712; c) C. Costentin, G. Passard, M. Robert, J.-M. Savéant, *Proceedings of the National Academy of Sciences* 2014, 111, 14990-14994; d) I. Azcarate, C. Costentin, M. Robert, J.-M. Savéant, *Journal of the American Chemical Society* 2016, 138, 16639-16644; e) Eva M. Nichols, J. S. Derrick, S. K. Nistanaki, P. T. Smith, C. J. Chang, *Chemical Science* 2018, 9, 2952-2960; f) E. Haviv, D. Azaiza-Dabbah, R. Carmieli, L. Avram, J. M. L. Martin, R. Neumann, *Journal of the American Chemical Society* 2018, 140, 12451-12456; g) A. Chapovetsky, M. Welborn, J. M. Luna, R. Haiges, T. F. Miller, S. C. Marinescu, *ACS Central Science* 2018, 4, 397-404; h) E. M. Nichols, C. J. Chang, *Organometallics* 2019, 38, 1213-1218; i) P. Sen, B. Mondal, D. Saha, A. Rana, A. Dey, *Dalton*

Transactions 2019, 48, 5965-5977; j) P. Gotico, B. Boitrel, R. Guillot, M. Sircoglou, A. Quaranta, Z. Halime, W. Leibl, A. Aukauloo, *Angewandte Chemie International Edition* 2019, 58, 4504-4509; k) A. Chapovetsky, J. J. Liu, M. Welborn, J. M. Luna, T. Do, R. Haiges, T. F. Miller Iii, S. C. Marinescu, *Inorganic Chemistry* 2020, 59, 13709-13718; l) C. G. Margarit, N. G. Asimow, M. I. Gonzalez, D. G. Nocera, *The Journal of Physical Chemistry Letters* 2020, 11, 1890-1895; m) P. Gotico, L. Roupnel, R. Guillot, M. Sircoglou, W. Leibl, Z. Halime, A. Aukauloo, *Angewandte Chemie International Edition* 2020, 59, 22451-22455; n) N. W. Kinzel, C. Werlé, W. Leitner, *Angewandte Chemie International Edition* 2021, 60, 11628-11686; o) S. Amanullah, P. Saha, A. Dey, *Journal of the American Chemical Society* 2021, 143, 13579-13592; p) C. Zhang, D. Drago, F. Brisset, B. Boitrel, B. Lassalle-Kaiser, W. Leibl, Z. Halime, A. Aukauloo, *Green Chemistry* 2021, 23, 8979-8987; q) A. Khadhraoui, P. Gotico, W. Leibl, Z. Halime, A. Aukauloo, *ChemSusChem* 2021, 14, 1308-1315; r) M. W. Drover, *Chemical Society Reviews* 2022, 51, 1861-1880; s) E. M. Johnson, J. J. Liu, A. D. Samuel, R. Haiges, S. C. Marinescu, *Inorganic Chemistry* 2022, 61, 1316-1326.

[8] a) C. Costentin, G. Passard, M. Robert, J.-M. Savéant, *Journal of the American Chemical Society* 2014, 136, 11821-11829; b) J. Bonin, M. Chaussemier, M. Robert, M. Routier, *ChemCatChem* 2014, 6, 3200-3207; c) J. Bonin, M. Robert, M. Routier, *Journal of the American Chemical Society* 2014, 136, 16768-16771; d) C. Costentin, M. Robert, J.-M. Savéant, A. Tatin, *Proceedings of the National Academy of Sciences* 2015, 112, 6882-6886; e) K. Guo, X. Li, H. Lei, W. Zhang, R. Cao, *ChemCatChem* 2020, 12, 1591-1595.

[9] N. Manoranjan, D. H. Won, J. Kim, S. I. Woo, *Journal of CO2 Utilization* 2016, 16, 486-491.

- [10] a) P. Gotico, Z. Halime, A. Aukauloo, Dalton Transactions 2020, 49, 2381-2396; b) E. Pugliese, P. Gotico, I. Wehrung, B. Boitrel, A. Quaranta, M.-H. Ha-Thi, T. Pino, M. Sircoglou, W. Leibl, Z. Halime, A. Aukauloo, Angewandte Chemie International Edition 2022, 61, e202117530; c) J. Derrick, M. Loipersberger, S. Nistanaki, M. Head-Gordon, E. Nichols, C. Chang, in ChemRxiv, 2022.
- [11] C. G. Margarit, C. Schnedermann, N. G. Asimow, D. G. Nocera, Organometallics 2019, 38, 1219-1223.
- [12] C. K. Williams, A. Lashgari, J. A. Tomb, J. Chai, J. J. Jiang, ChemCatChem 2020, 12, 4886-4892.
- [13] a) H. Rao, J. Bonin, M. Robert, ChemSusChem 2017, 10, 4447-4450; b) H. Rao, L. C. Schmidt, J. Bonin, M. Robert, Nature 2017, 548, 74-77; c) H. Rao, J. Bonin, M. Robert, Chemical Communications 2017, 53, 2830-2833.
- [14] A. Khadhraoui, P. Gotico, B. Boitrel, W. Leibl, Z. Halime, A. Aukauloo, Chemical Communications 2018, 54, 11630-11633.
- [15] a) S. Sung, D. Kumar, M. Gil-Sepulcre, M. Nippe, Journal of the American Chemical Society 2017, 139, 13993-13996; b) S. Sung, X. Li, L. M. Wolf, J. R. Meeder, N. S. Bhuvanesh, K. A. Grice, J. A. Panetier, M. Nippe, Journal of the American Chemical Society 2019, 141, 6569-6582.
- [16] C. Costentin, J.-M. Savéant, Journal of the American Chemical Society 2018, 140, 16669-16675.
- [17] a) B. M. Stratakes, J. L. Dempsey, A. J. M. Miller, ChemElectroChem 2021, 8, 4161-4180; b) C. Costentin, S. Drouet, M. Robert, J.-M. Savéant, Journal of the American Chemical Society 2012, 134, 11235-11242.

[18] S. Sinha, J. J. Warren, *Inorganic Chemistry* 2018, 57, 12650-12656.